

# Nanostructured Inorganic–Organic Composites as a Basis for Solid Polymer Electrolytes with Enhanced Properties

L. M. Bronstein, C. Joo, R. Karlinsey, A. Ryder, and J. W. Zwanziger\*

Department of Chemistry, Indiana University, Bloomington, Indiana 47405

Received February 19, 2001

A family of lithium electrolyte materials based on a polymer–inorganic hybrid is described. The base material is a blend of poly(ethylene oxide) and an organic–inorganic composite made from polyether-functionalized methoxysilanes and aluminum alkoxides. Lithium is incorporated through addition of a salt. The resulting materials are shown through a combination of methods, including transmission electron microscopy and solid-state NMR, to consist of an amorphous inorganic network, with nanoscopic voids, which stabilize the added polymer. The composite polymer electrolytes show good resistance to crystallization and good conductivity, as determined by differential scanning calorimetry and impedance measurements, respectively. The nanoscale structure of the underlying inorganic material is concluded to be responsible for the bulk properties of the system, especially those that differ from the properties of similar, pure salt-in-polymer electrolytes.

## 1. Introduction

Conventional solid polymer electrolytes (SPEs) are plagued with limitations, including modest conductivity, low cation transference numbers, and low electrochemical and mechanical stability. The prototypical SPE consists of poly(ethylene oxide) (PEO) and a lithium salt.<sup>1,2</sup> The glass transition temperatures of such SPEs are subambient, so that under routine operating conditions the material allows cation transport through the amorphous, liquidlike regions of the polymer.<sup>3</sup> Unfortunately such SPEs are prone to crystallization, and typically show cation transference numbers in the 0.1–0.3 range. These properties can be improved through plasticization, cross-linking, and other methods,<sup>4</sup> but the improvement usually comes at the expense of other important material parameters, such as mechanical strength and electrochemical stability. Nevertheless, the advantages of an SPE-based lithium battery, including low weight, small size, and improved safety, are such that solving these problems would have a significant impact.

Traditional polymer electrolytes consist of a salt dissolved in a polymer host. The salt supplies the mobile ions, and the polymer provides the bulk material properties, such as high compliance and formability. For a salt to dissolve in a polymer, the lattice energy of the salt must be overcome; this is accomplished by including coordinating functionalities in the polymer, to provide a large negative solvation energy, and by using salts with large, low-charge anions, to minimize the salt

lattice energy.<sup>3</sup> Thus, the prototypical salt-in-polymer systems use PEO  $[(-\text{CH}_2-\text{CH}_2-\text{O}-)]$  for the polymer and salts such as lithium triflate,  $\text{LiCF}_3\text{SO}_3$ . Crystal structures show that the ether oxygens coordinate the cations from the salt, and are separated by the optimum length of the alkane chain to permit formation of helical regions, which wrap around the cations.<sup>5,6</sup> In the amorphous state coordination appears to involve several neighboring polymer chains.<sup>7</sup> These regions permit 4–5 ether oxygens to have close contact with each cation. Other polyethers with longer or shorter alkane chains are less effective for cation transport. Other Lewis base groups, such as sulfur and nitrogen, can be substituted for oxygen. The ion conductivity typically shows a maximum at ratios of ether oxygen to cation in the range 8–14.

The polymer systems studied to date show striking differences in conductivity mechanism with inorganic fast ion conductors, due primarily to the mobility of the polymer chains. This is true even in the “polymer-in-salt” rubbers discovered by Angell, in which the polymer is only a minority constituent.<sup>8,9</sup> Near the glass transition, which is typically a bit below 0 °C in polymer electrolytes, these systems appear to have a heterogeneous structure of liquidlike amorphous regions interspersed with rigid glassy or crystalline domains. The cation mobility is much higher in the amorphous regions, where it is thought to be strongly correlated with motion of the polymer chains. This view has been quantified to some extent in the dynamic bond percola-

(1) Wright, P. V. *Br. Polym. J.* **1975**, *7*, 319.

(2) Abraham, K. M.; Alamgir, M. *Solid State Ionics* **1994**, *70/71*, 20.

(3) Shriver, D. F.; Bruce, P. G. Polymer electrolytes {I}: General principles. In *Solid State Electrochemistry*; Bruce, P. G., Ed.; Cambridge University Press: Cambridge, 1997; pp 95–118.

(4) Meyer, W. H. *Adv. Mater.* **1998**, *10*, 439.

(5) Lightfoot, P.; Mehta, M. A.; Bruce, P. G. *Science* **1993**, *262*, 883.

(6) Lightfoot, P.; Nowinski, J. N.; Bruce, P. G. *J. Am. Chem. Soc.* **1994**, *116*, 7469.

(7) Mao, G. M.; Saboungi, M. L.; Price, D. L.; Armand, M. B.; Howells, W. S. *Phys. Rev. Lett.* **2000**, *84*, 5536.

(8) Angell, C. A.; Liu, C.; Sanchez, E. *Nature* **1993**, *362*, 137.

(9) Angell, C. A.; Fan, J.; Liu, C.; Lu, Q.; Sanchez, E.; Su, K. *Solid State Ionics* **1994**, *69*, 343.

tion model of Ratner and colleagues, which provides a microscopic, statistical treatment of ion motion correlated with the polymer dynamics.<sup>10</sup>

Polymer composites have been developed recently that address these issues in different ways.<sup>4,11–13</sup> One approach is to cross-link the polymer, which suppresses crystallization and improves mechanical performance.<sup>4</sup> The disadvantage of this approach is that the  $T_g$  is raised, so that the conductivity at ambient temperatures is reduced. The cross-linked material can be additionally plasticized, but this typically requires such a high degree of plasticization that the resulting gels are of reduced electrochemical stability and much of the mechanical advantages are lost. Moreover, low molecular weight plasticizers such as simple carbonates, oligoethers, or tetraglyme can be lost from the SPE membrane during aging, eroding the SPE properties over time.

A different, synthetically challenging, approach is to graft ethylene oxide oligomers onto stiff polymer backbones.<sup>4</sup> This results in a layered architecture with excellent mechanical properties and suppressed PEO crystallization. A disadvantage of this approach is the marginal electrochemical stability of the resulting materials, which arises from the  $\pi$ -conjugated electronic structure of the poly(*p*-phenylene) used as the backbone. Polymer–inorganic intercalate materials provide another route to composites with promising electrochemical properties. These materials have the additional advantage of fixed Lewis acid sites, and therefore a high transference number for the cations (that is, conductivity is dominated by the cation, not the anion, motion). Such intercalates have been made with both the traditional PEO,<sup>12,14</sup> and also polyphosphazenes;<sup>15</sup> a problem with this approach is the anisotropy of the resulting conductivity. Since they appear to yield isotropic materials, the siloxaluminates synthesized recently by Shriver and colleagues represent a potentially major improvement on this approach.<sup>16,17</sup>

Scrosati and colleagues showed recently that the advantages of a Lewis acid-rich composite can be obtained by combining ceramic nanoparticles with PEO.<sup>18,19</sup> This work was done using alumina particles, but other inorganic nanoparticles can be used as well. While PEO crystallization is reduced in these systems, it seems to be so due to a kinetic mechanism. Therefore, questions remain about the long-term stability of materials prepared with this approach.

The composites discussed above all represent significant improvements over simple PEO/salt electrolytes.

(10) Ratner, M. A.; Nitzan, A. *Faraday Discuss. Chem. Soc.* **1989**, *88*, 19.

(11) Croce, F.; Appetecchi, G. B.; Persi, L.; Scrosati, B. *Nature* **1998**, *394*, 456.

(12) Giannelis, E. P. *Adv. Mater.* **1996**, *8*, 29.

(13) Quartarone, E.; Mustarelli, P.; Magistris, A. *Solid State Ionics* **1998**, *110*, 1.

(14) Lemmon, J. P.; Wu, J.; Oriakhi, C.; Lerner, M. M. *Electrochim. Acta* **1995**, *40*, 2245.

(15) Hutchison, J. C.; Bissessur, R.; Shriver, D. F. *Chem. Mater.* **1996**, *8*, 1597.

(16) Rawsky, G. C.; Fujinami, T.; Shriver, D. F. *Chem. Mater.* **1994**, *6*, 2208.

(17) Fujinami, T.; Tokimune, A.; Mehta, M. A.; Shriver, D. F.; Rawsky, G. C. *Chem. Mater.* **1997**, *9*, 2236.

(18) Croce, F.; Appetecchi, G. B.; Persi, L.; Scrosati, B. *Nature* **1998**, *394*, 456.

(19) Appetecchi, G. B.; Croce, F.; Persi, L.; Ronci, F.; Scrosati, B. *Electrochim. Acta* **2000**, *45*, 1481.

They are also not without their limitations: the simpler systems may suffer from a tendency to crystallize over long times, while the more complex systems appear to be difficult and expensive to prepare. Recently a family of nanostructured composite polymer electrolytes<sup>20</sup> were developed which appear highly promising as solutions to the problems listed above found in conventional SPEs. The heart of this new family is an organic–inorganic composite (OIC) consisting of a mesoporous aluminosilicate network tethered to polyether chains.<sup>21</sup> The polyether chains make this composite intimately compatible with PEO, while the aluminosilicate provides a stabilizing structure.<sup>22,23</sup> We presume that, due to this compatibility, the aluminosilicate network is able to penetrate the PEO phase, forming a scaffold for PEO chains coordinating Li salt. In the present paper we discuss the structure, mobility, and conductivity of such hybrid composites, and dependences of those characteristics on PEO molecular weight, material composition, and some other parameters.

## 2. Experimental Procedures

Poly(ethylene glycol) (PEG) and PEO with molecular weights of 600, 1000, 2000, 4600, 8000, and 100000, poly(ethylene oxide) dimethyl ether ( $M_n = 2000$ ), and poly(ethylene glycol) methyl ether ( $M_n = 2000$ ) were purchased from Aldrich and used as received. Lithium triflate, THF, aluminum tri-*sec*-butoxide (Aldrich), chloroform (EM Industries, Inc.), and (3-glycidylpropyl)trimethoxysilane (GLYMO; Fluka) were used without further purification. Water was purified with a “Barnstead NANOpure water” purification system.

Synthesis of an organic–inorganic composite based on PEO (OIC–PEO) was carried out by a procedure described elsewhere<sup>1,2</sup> using several modifications. In a typical experiment, 0.4 g (9 mmol) of PEO in 5 mL of chloroform was mixed with 0.1 g (0.64 mmol) of lithium triflate in 5 mL of THF. After 30 min of stirring, the solution was kept aside. The inorganic part of the hybrid was prepared by hydrolysis of the mixture of GLYMO with aluminum tri-*sec*-butoxide in a molar ratio of 80:20, respectively. Hydrolysis was initiated by addition of 15% of an equimolar amount of water containing HCl (0.01 N solution). After 15 min of stirring at 0 °C (water–ice bath) and 15 min at room temperature, the reaction mixture was charged with the residue of the 0.01 N HCl solution and stirred for 20 min. The prehydrolyzed sol was added to the solution containing PEO and Li salt (the amount was determined by the desired ratio of PEO to inorganic hybrid, which varied in the range of 30–70 wt %) and stirred for 1 h. Afterward the solvents were evaporated on a Teflon dish at 65–70 °C for 1 h. The solid film was treated at 130 °C in a vacuum for 1 h to complete condensation. Films were easily removed from the dish and ready for examination. Samples were sealed and stored in a desiccator. By thermogravimetric analysis (TGA) in N<sub>2</sub> (5 °C/min), the weight loss from apparent water (up to 150 °C) did not exceed 0.5%.

Differential scanning calorimetry (DSC) was performed with a Perkin-Elmer DSC 7 with liquid N<sub>2</sub> as a coolant. Samples ranged from 6 to 16 mg in weight, and were sealed in reusable stainless steel high-pressure capsules. The polymer sample was cooled to –85 °C and then heated to 120 °C. The glass transition and melting transition temperatures ( $T_g$  and  $T_m$ ) were measured, and the associated enthalpy changes ( $\Delta H$ ) calculated.

(20) Ulrich, R.; Zwanziger, J. W.; De Paul, S. M.; Richert, R.; Wiesner, U.; Spiess, H. W. *Proc. ACS Div. PMSE* **1999**, *80*, 610.

(21) Templin, M.; Wiesner, U.; Spiess, H. W. *Adv. Mater.* **1997**, *9*, 814.

(22) Templin, M.; Franck, A.; Du Chesne, A.; Leist, H.; Zhang, Y.; Ulrich, R.; Schädler, V.; Wiesner, U. *Science* **1997**, *278*, 1795.

(23) De Paul, S. M.; Zwanziger, J. W.; Ulrich, R.; Wiesner, U.; Spiess, H. W. *J. Am. Chem. Soc.* **1999**, *121*, 5727.

Transmission electron microscopy (TEM) images were acquired on a Zeiss EM 912 $\Omega$  at an acceleration voltage of 120 kV. Samples were ground in a ball mill and suspended in acetone. One droplet of the suspension was applied to a 400 mesh carbon-coated copper grid and left to dry in air.

Nitrogen sorption experiments were carried out using a Micromeritics Gemini instrument. Samples were degassed at 100 °C in vacuo for 12 h prior to investigation.

Conductivity was measured as follows. All samples were vacuum-dried at 50 °C overnight to minimize the effects of residual water absorption. Sample thickness was determined using a micrometer, and ranged between 200  $\mu\text{m}$  and 1 mm. Gold contacts of area 0.0647  $\text{cm}^2$  were attached directly to the polymer films by means of a Polaron E5100 sputter coater. Due to the flexible nature of the polymer films, slight modifications were made to the sputter chamber to reduce gold penetration into the films. Sputtering was accomplished in 1 min, and during this time the samples were held between -10 and -15 °C, as monitored with a thermocouple. After gold electrodes were attached, each sample was placed into a measurement rig and attached to a Hewlett-Packard 4192A impedance analyzer. The oscillation level of the applied pulse was 1 V over a frequency range of 5 Hz to 13 MHz. The samples were modeled to a parallel circuit comprised of a resistor and capacitor. Admittance data were recorded using this circuit model and subsequently converted to obtain impedance plots.

Solid-state NMR measurements were performed on a Bruker DMX 400 MHz NMR spectrometer, using a 4 mm magic angle sample spinning probe. Rotation frequencies are indicated on the spectra shown and were stabilized with an active feedback spin-rate controller.

### 3. Results

Table 1 summarizes the samples studied here, including their composition and results from calorimetry and conductivity measurements. Figure 1 shows the TEM image of a calcined sample, used to estimate the inorganic structure in the composite material. Figure 2 shows a typical set of one-dimensional NMR experiments on  $^{13}\text{C}$ ,  $^{29}\text{Si}$ , and  $^{27}\text{Al}$ , performed to determine the distribution of chemical sites. Figure 3 shows the  $^{27}\text{Al}$  two-dimensional multiple-quantum magic angle spinning (MQ-MAS) correlation spectrum obtained from a representative sample, done to resolve the overlapping aluminum resonances. Figure 4 shows a two-dimensional proton-carbon correlation experiment, performed to assess local dynamics. Figure 5 shows complex impedance data, and the fit used to extract the sample resistance and hence derive conductivity. The interpretation of these results is discussed in detail in the next section.

### 4. Discussion

The method described in the Experimental Procedures permits the preparation of free-standing composite films over a wide range of molecular weights and material compositions. The mechanical modulus of the formulations tested so far shows the expected sharp decrease at the glass transition followed by a gradual increase with temperature up to the rubber transition, indicating an entropy-dominated modulus and, of practical importance, strength which does not degrade through the temperature range of application.<sup>24</sup>

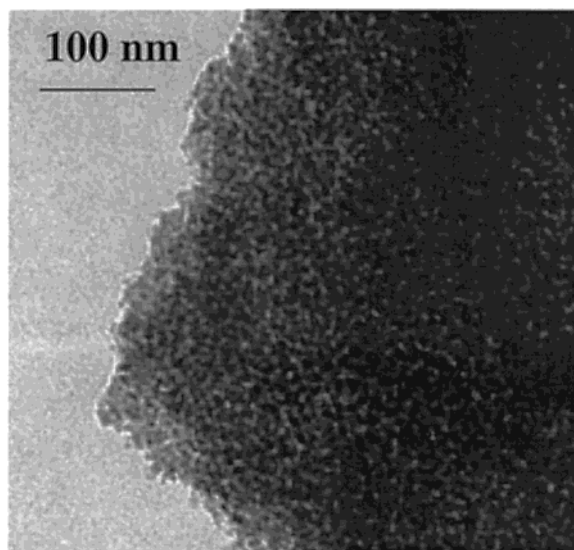


**Figure 1.** TEM image of the mesoporous aluminosilicate network present after calcination of OIC-PEO based on PEG-8000 and 70% inorganic component. This network stabilizes the polymer such that crystallization is suppressed while the local segmental motions that promote ion conductivity remain. The size scale of the pores as estimated both by nitrogen adsorption and by NMR experiments is roughly 3–10 nm.

**4.1. Structure: Microscopy.** To determine the overall structure of OIC-PEO based on PEO and aluminosilicates, the sample derived from PEO-8000 and containing 70% inorganic phase was subjected to calcination at 500 °C in  $\text{O}_2$ . This procedure removes the organic components, while leaving the inorganic structure practically unaffected.<sup>25</sup> The TEM image of the calcined sample (Figure 1) shows a highly porous material made up of an interpenetrating inorganic network. The  $\text{N}_2$  adsorption isotherms for this inorganic network are similar to those obtained for materials with both meso- and micropores, which is characteristic of metal oxides templated over nonionic surfactants or block copolymers.<sup>25,26</sup> In the case of PEO templating, the material structure strongly depends on the amount of organic template and its molecular weight and varies from completely microporous (20–27% PEO-10000) to partially mesoporous (33–43%).<sup>26</sup> In our case, the noticeable mesoporosity at 30 wt % PEO template can be explained by the preparation technique: slow evaporation of solvents from reaction solution (before final condensation of the inorganic network) results in aggregation of PEO chains. This material contains a significant fraction of mesopores, in which BJH pore diameters vary from 3 to 10 nm. The low BET surface area (125  $\text{m}^2/\text{g}$ ) could be attributed to the low fraction of micropores formed by individual PEO chains.

**4.2. Structure: Solid-State NMR.** The local structure of the inorganic hybrid material was studied with solid-state NMR. The carbon, silicon, and aluminum magic angle spinning (MAS) spectra are shown in Figure 2 for a representative composition: MW 8000 PEO and 55% added inorganic modifier. Other compositions show similar spectra. The carbon spectrum shows

(25) Göltner, C. G.; Henke, S.; Weissenberger, M. C.; Antonietti, M. *Angew. Chem., Int. Ed. Engl.* **1998**, *37*, 613.

(26) Göltner, C.; Smarsly, B.; Berton, B.; Antonietti, M. *Chem. Mater.*, in press.

(24) Ulrich, R.; Zwanziger, J. W.; De Paul, S. M.; Reiche, A.; Leist, H.; Wiesner, U.; Spiess, H. W. To be submitted for publication.

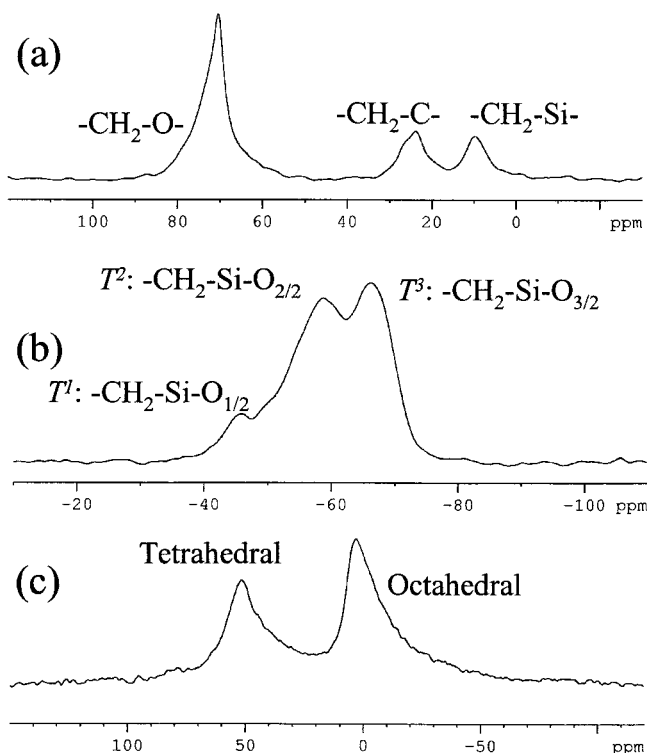


**Figure 2.** MAS spectra of the OIC sample derived from MW 8000 PEG and 55% aluminosilicate component: (a) carbon-13; (b) silicon-29; (c) aluminum-27. The assignments are discussed in the text.

three resonances, assigned to  $-\text{C}-\text{O}-$  linkages (70 ppm),  $-\text{CH}_2-$  groups (20 ppm), and  $-\text{C}-\text{Si}-$  units (9 ppm). These groups are all expected on the basis of the synthesis,<sup>21,23</sup> and are useful for further characterization as discussed below. The silicon spectrum shows a distribution of so-called  $T^n$  groups, indicating  $-\text{C}-\text{Si}(\text{OH})_{3-n}\text{O}_{n/2}$  units.<sup>21,23</sup> These units include  $n$  bridging connections through oxygen to other parts of the network and one carbon linkage, and the remaining binding sites are occupied presumably by  $-\text{OH}$  units. The significant populations of  $T^3$  groups indicate a high degree of three-dimensional network character of the inorganic hybrid in the polymer electrolyte. The aluminum spectrum shows two distinct sites at 0 and 65 ppm, indicating octahedral and tetrahedral coordination, respectively. Both sites show substantial broadening to the high-field side, typical of local disorder and large quadrupole couplings. To investigate the aluminum sites further, we recorded the MQ-MAS of selected samples; the result for the sample containing MW 8000 PEO and 55% inorganic additive is shown in Figure 3. This experiment<sup>27</sup> yields an isotropic–anisotropic correlation and hence separates the spectra of different aluminum sites, which would overlap in one-dimensional experiments. The spectra show that there are no five-coordinate aluminum species (which would be obscured between the octahedral and tetrahedral sites in one dimension) and that indeed both sites show significant disorder, as evidenced by their broad two-dimensional line shapes. The above results are consistent with the picture of the structure including a three-dimensional inorganic-based network, polyether-linked

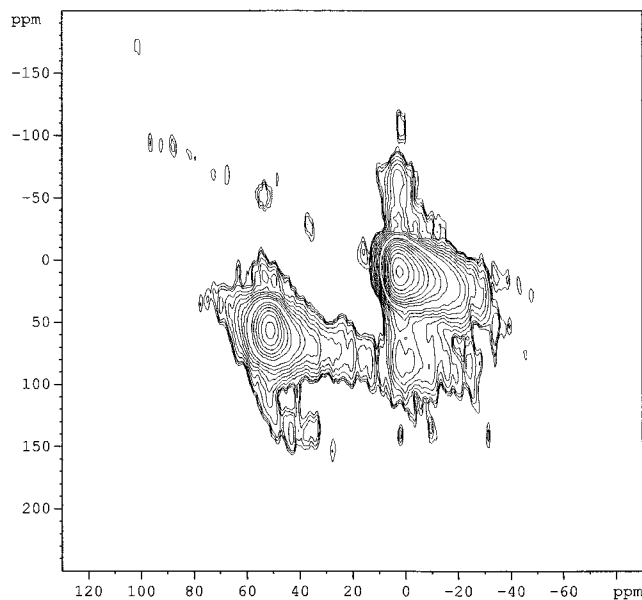


**Figure 3.** MQ-MAS spectrum of aluminum in the OIC sample derived from MW 8000 PEG and 55% aluminosilicate component. Both axes are aluminum shifts. This experiment resolves resonances from quadrupolar nuclei that overlap in one-dimensional MAS. The spectrum shows that both the octahedral and tetrahedral sites are distorted (particularly the latter) and that there are no additional sites that were masked in the one-dimensional spectra.

silanes bridged by oxide bonds, and aluminum present roughly equally in tetrahedral and octahedral coordination. The presence of tetrahedral Al ( $\text{AlO}_4^-$  species) is speculated to be responsible for the high Li transference numbers for this material, which reach 0.7.<sup>20</sup> These four-coordinate species can improve transport of Li cations through the OIC, perhaps by providing additional coordination sites that break up ion pairs and triplets.

**4.3. Dynamics: Calorimetry.** The conductivity of polymer electrolytes containing Li salts is determined by the content and mobility of the Li ions within the polymeric matrix. The mobility is governed by two major factors: the mobility of the polymer, and the interaction of Li cations with anions. In the present composite materials, there are two sources of anions: triflate ions, the amount of which exactly matches the Li content in each sample, and tetrahedral  $\text{Al}^-$  species, the quantity of which can vary depending on the fraction of inorganic network in the composite. Mobility within the PEO also depends on at least two parameters: mobility in the amorphous phase, which is grossly characterized by the  $T_g$ , and the amount of crystalline phase. For pure PEO, the crystalline fraction is normally determined by the polymer molecular weight. Starting from MW 1000, the degree of crystallinity is about 90%, while in high molecular weight polymers (100000 and above) the degree of crystallinity is about 50% and the  $T_g$  is about  $-52^\circ\text{C}$ .<sup>28</sup> Poly(ethylene glycols) with molecular weights below 1000 are liquids. The  $T_g$  values, melting temperatures, and enthalpy changes ( $\Delta H$ ) for the present OIC–PEO materials are presented in Table 1. As might be expected, samples derived from PEO-600 are amorphous, regardless of OIC content, and a display slightly

(27) Frydman, L.; Harwood, J. S. *J. Am. Chem. Soc.* **1995**, *117*, 5367.

(28) *Polymeric Materials Encyclopedia*; Salamone, J. C., Ed.; CRC Press: Boca Raton, FL; New York, 1996; Vol. 8, p 6039.

Table 1<sup>a</sup>

sample notation	PEO MW	inorganic component fraction, wt %	$T_g$ , °C	$T_m$ , °C	$\Delta H$ , J/g	degree of crystallinity, %	$\sigma$ , S/cm
L6-30	600	30	-56			0.0	
L6-40	600	40	-54			0.0	$2.95 \times 10^{-5}$
L6-55	600	55	-52			0.0	$1.76 \times 10^{-5}$
L6-70	600	70	-42			0.0	$2.81 \times 10^{-6}$
L10-55	1000	55	-49	30	0.35	0.3	$8.47 \times 10^{-6}$
L20-55	2000	55	-44	38	45.9	44	$5.73 \times 10^{-6}$
L20DM-55 <sup>b</sup>	2000	55	-46	44	25.8	25	$2.80 \times 10^{-5}$
L20M-55 <sup>c</sup>	2000	55	-38	47	17.0	16	$2.82 \times 10^{-5}$
L46-55	46800	55	-47	45	38.2	37	$5.72 \times 10^{-6}$
L80-55	8000	55	-44	44	16.8	16	$2.66 \times 10^{-5}$
L1000-55	100000	55	-39	42	13.2	13	$3.79 \times 10^{-5}$
L80-30	8000	30	-54	41	47.2	30	$1.15 \times 10^{-5}$
L80-70	8000	70	-40			0.0	$3.61 \times 10^{-6}$
L1000-70	100000	70	-34	47	3.3	5	$5.61 \times 10^{-6}$

<sup>a</sup> The sample notation (column 1) gives in abbreviated form the PEO molecular weight (column 2) and the weight percent of the inorganic component (column 3). For each sample, the glass transition temperature  $T_g$  and the temperature of any observed PEO melting event  $T_m$  are given (columns 4 and 5). The heat flow due to the melting event is given in column 6; this number is indicative of the extent of PEO crystallization present in each sample. Column 7 gives the degree of crystallinity, estimated from  $\Delta H_{PEO(8000)} = 240$  J/g (90% crystalline phase) and the PEO content in each sample. Finally, column 8 gives the conductivity at 20 °C. <sup>b</sup> PEO dimethyl ether was used. <sup>c</sup> PEG methyl ether was used.

lower  $T_g$  than is typical for high molecular weight PEO. The increase of the inorganic component fraction (from 30 to 70 wt %) for the PEO-600 series results in the monotonic increase of the  $T_g$  from -56 to -42 °C. The increase of the molecular weight of PEO (at constant 55 wt % inorganic component) also results in the increase of the  $T_g$ , though the L20-55 sample, which is characterized by the highest crystallinity, is exceptional. For the PEO-8000 series, the  $T_g$  also depends on the inorganic component amount. At the same time, the crystalline fraction, which is comparatively high for the L80-30 sample, is suppressed when the fraction of inorganic component increases to 70%. A similar dependence was observed for organic-inorganic hybrid materials derived from PEO and SiO<sub>2</sub>.<sup>29</sup> This dependence can be explained by an increase in the amount of inorganic network nodes in the material and by a consequent decrease of the PEO chain length between these nodes, which prevents chains from free packing. In all samples, any crystalline fraction reappears after melting (at 80 °C) only very slowly, over a 1 week period. This observation is explained by the slow relaxation process of the PEO chains, which are located within the inorganic network.

In the literature, the influence of hydroxyl end groups on crystallization of PEG is not quite clear,<sup>30,31</sup> and both effects of -OH group interaction and incorporation of bulkier groups are discussed in terms of their influence on polymer crystallinity. Hydroxyl groups can provide additional interactions between polymer chains due to hydrogen bonding, while diminishing mobility of the amorphous PEO phase. On the other hand, in the current OIC-PEG materials, end groups can interact with GLYMO, thus providing tethering of the PEO chains to the inorganic network. To scrutinize the influence of OH groups, we compared OIC samples based on PEG-2000, PEO-2000 dimethyl ether, and PEG-2000 methyl ether. As can be seen from Table 1, replacement of one or both hydroxyl groups of PEG with

methoxy groups decreases the crystallinity. Because suppression of crystallinity successfully occurs for both samples (dimethyl and monomethyl ether), one can surmise that crystallinity is enhanced when both ends of a PEG chain of a given molecular weight can interact either with other PEG end groups or with GLYMO residues. In the OIC-PEO samples the amount of hydroxyl groups is undetectable in the NMR spectra but is certainly not rigorously zero.

**4.4. Dynamics: Solid-State NMR.** While calorimetric experiments help assess the global dynamics of the material, solid-state NMR is useful as a probe of local dynamics. We used the wide-line separation of interactions experiment<sup>32,33</sup> (WISE) to correlate the atomic dynamics, as judged from the proton NMR line widths, with their chemical sites. In this experiment, the protons are excited and the magnetization evolves for an initial time  $t_1$ . This magnetization is then transferred to carbon for detection, under moderate magic angle spinning conditions. The resulting two-dimensional spectrum yields the proton spectra sorted by the identity of the carbon atoms to which each is bound.<sup>23</sup>

Figure 4 shows the WISE spectrum of the sample derived from MW 8000 PEO and 55% inorganic component, at 0 °C (well above the glass transition temperature of -44 °C). Shown also are slices representing the proton spectra at the chemical shifts of the three carbon resonances. The proton spectrum associated with the 70 ppm carbon peak shows a marked two-component character, which includes both a narrow component (8 kHz full width at half-maximum), indicating significant mobility, and a broad component (50 kHz), indicating static sites. These protons are associated with carbon in -CH<sub>2</sub>-O- units, and there are two sources of such carbon: the PEO polymer, and the polyether component of the organic-inorganic hybrid. Conversely, the proton spectra associated with the carbon resonances at 20 and 9 ppm are both relatively broad (37 kHz), indicating static sites. These carbon resonances are due to methylene and silane carbons, respectively, both of which are

(29) Jiang, S.; Yu, D.; Ji, X.; An, L.; Jiang, B. *Polymer* **2000**, *41*, 2041.

(30) Ba, H.; Peng, X.; Chen, D.; Wang, F. *Chin. J. Polym. Sci.* **1992**, *10*, 32.

(31) Preechatiwong, W.; Schultz, J. M. *Polymer* **1996**, *37*, 5109.

(32) Zumbulyadis, N. *Phys. Rev. B* **1986**, *33*, 6495.

(33) Schmidt-Rohr, K.; Claus, J.; Spiess, H. W. *Macromolecules* **1992**, *25*, 3273.

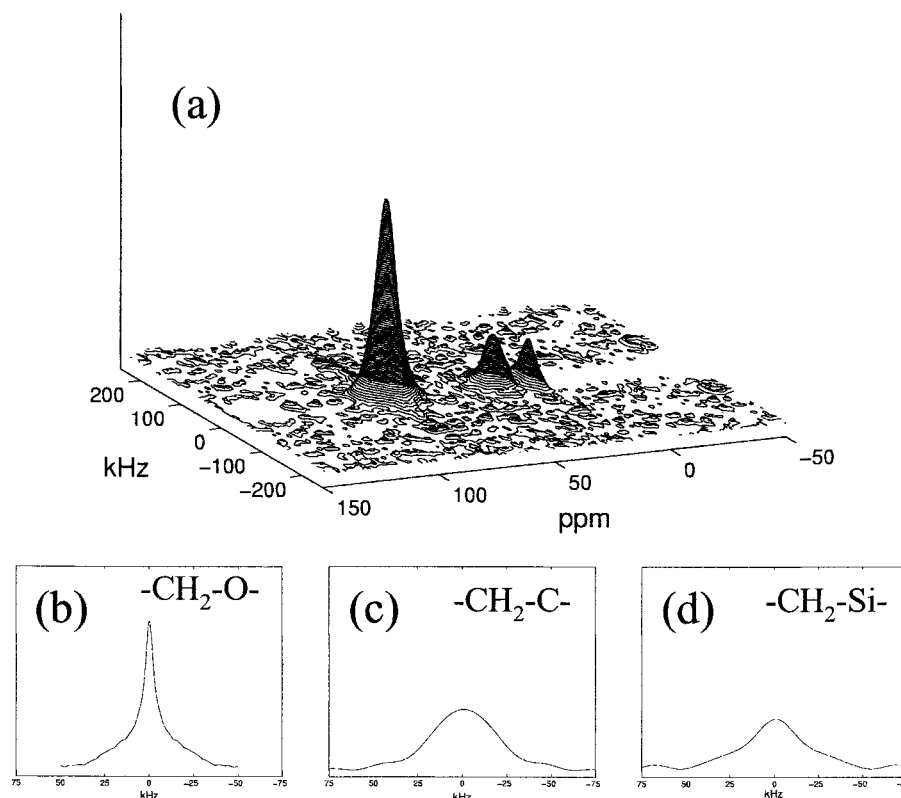


**Figure 4.** (a) WISE NMR spectrum of the OIC sample derived from MW 8000 PEG and 55% aluminosilicate component. Front axis: carbon shift (ppm). Left axis: proton line width (kHz). (b)–(d) Proton spectra extracted from the WISE spectrum by taking slices at the three dominant carbon shifts. (b) reflects protons bound in  $-\text{CH}_2\text{-O}-$  units, and shows both slow and fast dynamic components. (c) reflects protons in alkyl methyl units, and (d) reflects protons in  $-\text{CH}_2\text{-Si}-$ . The breadth of the latter two signals indicates that the OIC network material is relatively rigid.

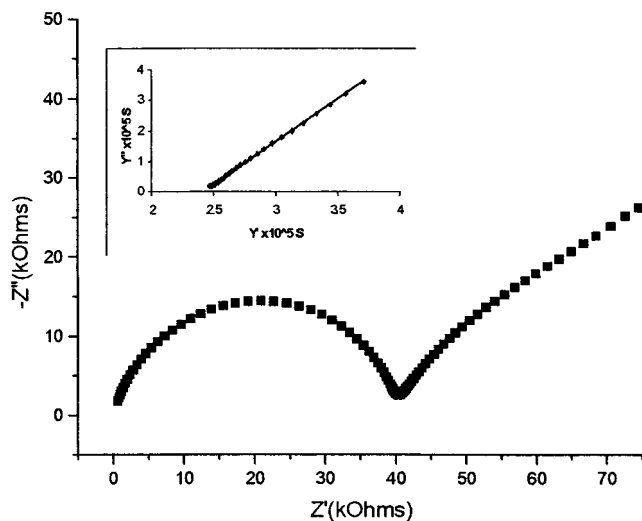


**Figure 5.** Room-temperature impedance data for the OIC sample based on PEG-600 and 55% inorganic component obtained by modeling a circuit to a resistor and capacitor in parallel. The sample resistance was determined through a linear fit of admittance data corresponding to the characteristic arc generated in a complex-plane plot, as shown in the inset. Data correspond to frequencies in the range 5 Hz to 13 MHz.

present solely in the organic–inorganic hybrid. We interpret these data as showing that the polymer, although confined by the nanopores of the organic–inorganic hybrid, remains relatively mobile above the glass transition, while the hybrid additive itself is relatively static. This result helps to explain why the hybrid material remains a good ion conductor even

though its strength is increased relative to that of pure salt-in-polymer formulations.

**4.5. Dynamics: Conductivity.** One can see (Table 1) that an increase of the inorganic component fraction strongly decreases the conductivity of the material, while an increase of the molecular weight of PEO influences the conductivity only through the amount of crystalline phase: when the degree of crystallinity increases, the conductivity decreases (L20-55 and L46-55). The comparison of DSC and conductivity data for all the samples shows that there is no obvious dependence between the  $T_g$  and conductivity, while the crystalline phase fraction and conductivity are closely connected. Probably, for all the samples, the  $T_g$  is sufficiently low, so the mobility of the PEO phase at room temperature is high. On the other hand, for the most crystalline samples, L20-55 and L46-55, the conductivity is lower than that for less crystalline samples at the same OIC content.

## 5. Conclusions

The family of materials discussed here, based on an organic–inorganic composite composed of an aluminosilicate network functionalized with polyethers and blended with poly(ethylene oxide), forms the basis for a series of lithium ion conductors with superior properties as compared to conventional salt-in-polymer electrolytes. We showed by a combination of TEM, NMR, and DSC that the inorganic component largely suppresses the crystallization of the polymer, which plagues simple polymer electrolytes, and that the inorganic

component forms a network with voids on the 10 nm size scale. These voids evidently stabilize the polymer in the amorphous, rubbery state, without substantially degrading its mobility. The presence of the polyethers on the surface of the inorganic material should aid both in blending with the polymer, and, importantly, in stabilizing the material against degradation with age via component separation. The conductivity of the composites is comparable to that found in simple polymer electrolytes, and is best for low molecular weight polymers and minimal added inorganic material. The presence of the anionic four-coordinate aluminum species is likely key to adding to enhancement of the lithium ion transference number,<sup>20</sup> and it is likely that single-

ion conductors can be made starting from the organic-inorganic composite used here.

**Acknowledgment.** This work was supported by a grant from the Petroleum Research Fund. L.M.B. thanks Professor Markus Antonietti and Sebastian Polarz at the Max Planck Institute on Colloids and Interfaces for help with TEM. J.W.Z. gratefully acknowledges valuable interactions with Professor Hans Spiess and his group at the Max Planck Institute for Polymer Research, including Dr. Uli Wiesner, Dr. Ralph Ulrich, and Dr. Susan De Paul.

CM011066B